MIT Libraries | DSpace@MIT

MIT Open Access Articles

Design Method for Buckling Amplified Piezoelectric Actuator Using Flexure Joint and its Application to an Energy Efficient Brake System

Massachusetts Institute of Technology

DSCC2012-MOVIC2012-8711

DESIGN METHOD FOR BUCKLING AMPLIFIED PIEZOELECTRIC ACTUATOR USING FLEXURE JOINT AND ITS APPLICATION TO AN ENERGY EFFICIENT BRAKE SYSTEM

Shinichiro Tsukahara, James Torres, Devin Neal and H. Harry Asada
Mechanical Engineering Department
Massachusetts Institute of Technology
Cambridge, MA 02139
{ tsukahar, jtorres9, dneal, asada }@mit.edu

ABSTRACT

This paper shows a practical design method for a displacement amplification mechanism for a piezoelectric actuator which employs a buckling-like phenomenon. This mechanical singularity realizes a substantial displacement magnification, at least 50 times, within a simple structure. An SMA preload mechanism essentially provides potential for full range push-pull actuation to the piezoelectric actuator. This integrated actuator performs a high energy transfer ratio and is suitable for brake mechanisms due to their requirement of high force, specific displacement and energy efficiency. A practical design method is shown and is evaluated by comparing the analytical model with finite element analysis and experimental hardware performance. The actuator properties obtained by these methods fit well each other with errors less than 13%.

The experimental actuators are applied to a brake for a commercial motor and its properties are evaluated. The brake can produce more than 2.5Nm in the displacement range of 0.5mm. These experimental results suggest that this novel piezoelectric actuator has potential for use in a wide range of applications.

INTRODUCTION

Energy efficiency is a major concern these days. Energy efficiency not only reduces energy consumption, but also affects the crucial value of various products. For example, more efficient motors require smaller energy reservoirs which result in enhanced performance, especially in mobile machines such as cars and robots. Electro-magnetic (EM) motors are arguably the most popular actuators in many machines. Their properties are based on the inductive energy transformation principle, which suits work conditions which need continuous motion regardless of force outputs required. EM motors consume energy depending on the output force regardless of their mechanical work. Hence, in load conditions which require

force output without motion, EM motors transmit no energy to the mechanical output, but still consume a significant amount of energy due to the electric resistance. Counter forcing mechanisms, such as masses and cylinders, not only possibly degrade the dynamic property of machines due to their additional masses, compliances and viscosities, but also make increase the size and weight of machines.

In contrast, piezoelectric actuators can produce constant force in static conditions without energy consumption due to their capacitive energy transformation principle. This suggests that piezoelectric actuators are adequate for vertical positioning and forcing applications which have load conditions requiring continuous force without continuous motion. In addition, piezoelectric actuators have high force density compared to permanent magnet motors and high bandwidth sufficient for most machines. However, piezoelectric actuators themselves can only generate displacements less than 0.2% of their length. For this reason, mechatronics researchers have focused on how to amplify the displacement of piezoelectric actuators.

Ultrasonic motors are the most commercially available method of magnification converting oscillatory piezoelectric motion to an axial continuous motion. They can drive at velocities comparable to EM motors. But their energy transformation depends on friction forces, which causes the risk of the output force varying based on the conditions and limits the utilization of the maximum force of piezoelectric actuators. Hydrostatic cylinders driven by piezoelectric pumps can also obtain reliable open-ended stroke actuation generated by a repetitive piezoelectric motion, but the energy transformation from piezoelectric actuator to oil has limited efficiency due to the elasticity and viscosity of oil. These types of magnification methods have potential for a wide range of applications requiring continuous motion, but detract from the force density.

Copyright © 2012 by ASME

There are several leverage mechanisms which amplify the displacement of piezoelectric actuators geometrically. The simplest of which is a lever mechanism that employs flexures as joints [1]. Another is a cymbal shape mechanism known as "Moony" [2] or "Rhombus" [3, 4]. These also use flexures as joints. The amplification ratio of each of these designs is typically limited to less than a factor of 10, because of the compliance of the mechanisms [5]. For these reason, multi-stage magnification is applied if higher amplification is required for the mechanisms [6, 7]. A buckling type mechanism was proposed as one kind of the geometric displacement magnification mechanisms which has a remarkably high magnification ratio typically around 50 and reaching up to 200 [8, 9].

The energy transformation ratios of all of these leverage magnification mechanisms utilizing flexures as joints depend highly on the compliance properties of the whole mechanism, especially of the flexure joints. The buckling type has fewer flexures, so the mechanism has a high potential to realize the high energy transformation ratio and displacement magnification ratio simultaneously. But the practical properties and design methods are not studied in conventional studies.

In addition to this mechanism, we apply shape memory alloy (SMA) as a preloading mechanism [9]. Some types of SMAs are also used as actuators, but we apply a superelastic type of SMA as a static force source. Compressive preloading is a typical method for piezoelectric actuators for achieving tensile actuation from piezoelectric actuators without applying tensile loads to piezoelectric stacks. Appropriate preloading provides the actuator with not only both compressive and tensile actuation but also enhancement of the piezoelectric effect [10, 11].

Some types of piezo brakes are presented conventionally focusing on the energy efficiency of piezoelectric actuators. Most of them employ some kinds of displacement amplification mechanisms [12, 13, 14]. Targeting EM motors, the hydrostatic amplification [14] can have sufficient properties but is hard to apply because of the need for maintenance. In contrast, the conventional geometric methods [12] don't need maintenance with adequate flexure design, but have limited displacement performance properties which can't substantially compensate for the wear at the brake plates for commercial products. Our buckling type actuator has potential to satisfy the specifications of commercial products due to their potential high energy transfer rate.

We present a practical design method for the buckling type piezoelectric actuator preloaded by SMA in this paper. Additionally, included are experimental results of the actuator designed along the methods shown. We applied the actuator to a brake for a commercial EM motor. Finally, experimental performance characteristics of the piezoelectric brake are shown.

DESIGN CALCULATIONS FOR BUCKLING AMPLIFICATION MECHANISM

Basic property

A conceptual configuration of the buckling type displacement amplification mechanism is shown in Fig. 1. Assuming ideal solid parts and ideal joints, the amplification ratio R with respected to the joint angle is obtained by Eq. (1) and is shown in Fig. 2.

$$R = \frac{dy}{dz} = \frac{dy}{d\theta} \Big/ \frac{dz}{d\theta} = L \sec^2 \theta / L \tan \theta \sec \theta = \csc \theta \quad (1)$$

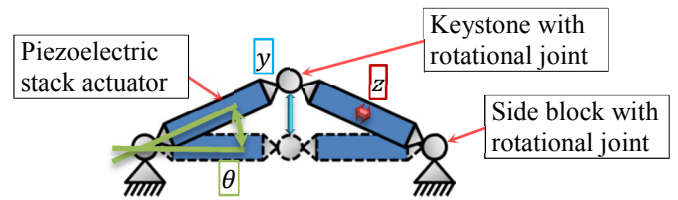$$\text{where} \begin{cases} y = L \tan \theta \\ z = L(\sec \theta - 1) \end{cases}$$

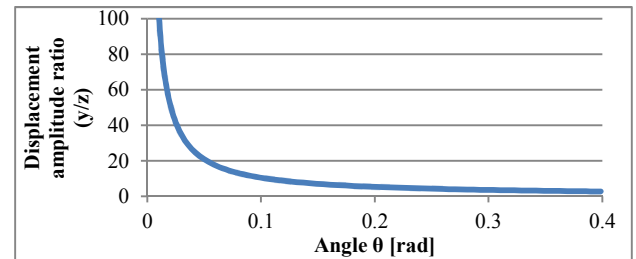FIGURE 1. BASIC ARCHITECTURE OF BUCKLING ACTUATOR

FIGURE 2. DISPLACEMENT AMPLIFICATION RATIO OF BUCKLING ACTUATOR

Due to the singularity, infinite amplification occurs at the zero angle/displacement configuration. In the proximity of the singular point, much higher amplification ratios comparing to other one-step leverage mechanism [15] can be obtained by this configuration.

Employing flexures as rotational joints, a low order mechanical model of the mechanism can be described as in Fig. 3, where each piezoelectric actuator is described as the combined function of a spring, k_P, and a force source, F_P, in parallel, compressive compliances of two joints attached on each piezoelectric actuator are assumed as a spring for each, k_J, and so are joint the rotational compliances, k_θ. The mechanical potential energy equation of this system is,

Copyright © 2012 by ASME

$$U = \frac{1}{2}k_\theta\theta^2 + \frac{1}{2}k_J z_J^2 + \frac{1}{2}k_B z_B^2 + \frac{1}{2}k_P z_P^2 + F_P z_P$$

$$= \frac{1}{2}k_\theta\theta^2 + \frac{1}{2}k_z z^2 + F_P z_P \qquad (2)$$

where $k_Z = \left(\frac{1}{k_J} + \frac{1}{k_P} + \frac{1}{k_B}\right)^{-1}$, $z = z_J + z_B + z_P$

Referring to Fig. 3, the following geometric relations as functions of y can be obtained.

$$\theta = \arctan\frac{y}{L}, \quad z = -L + \sqrt{L^2 + y^2} \qquad (3)$$

Regarding Eq. (3), output force can be obtained by differentiation of Eq. (2) to obtain Eq. (4). Each stiffness coefficient is mentioned later.

$$F_y = -\frac{dU}{dy} = -k_\theta\theta\frac{d\theta}{dy} - k_z z\frac{dz}{dy} - F_P\frac{dz_P}{dy}$$

$$= -k_\theta\frac{L}{L^2+y^2}\left(\arctan\frac{y}{L}\right) - k_z y\left(1 - \frac{L}{\sqrt{L^2+y^2}}\right) \qquad (4)$$

$$-\frac{k_z}{k_P}F_P\frac{y}{\sqrt{L^2+y^2}}$$

$$\approx -k_\theta\frac{y}{L^2+y^2} - k_z y\left(1 - \frac{L}{\sqrt{L^2+y^2}}\right) - \frac{k_z}{k_P}F_P\frac{y}{\sqrt{L^2+y^2}}$$
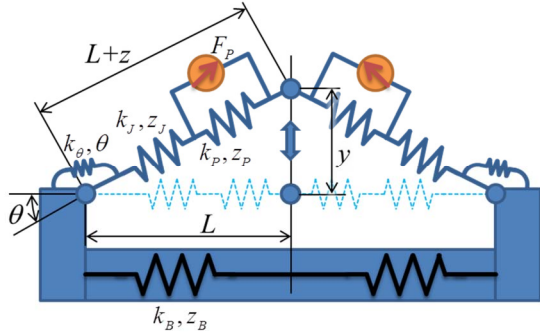

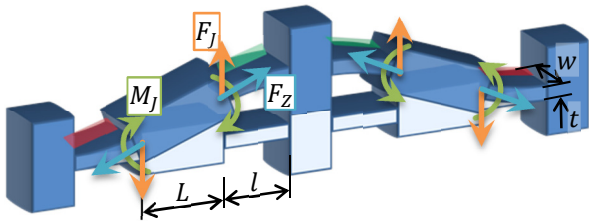FIGURE 3. LOW ORDER MECHANICAL MODEL OF FLEXURE BUCKLING ACTUATOR

FIGURE 4. FORCE BALANCE OF PIEZOELECTRIC STACK

Compliance properties

Considering loads taken to the center part described in Fig. 4, rotational load equilibrium is obtained as Eq. (5).

$$2M_J = LF_J \qquad (5)$$

Round filets are utilized to remove stress concentrations at the ends of the flexure joints. As a result, compliance properties of the pair of filets on each flexure beam for both bending $k_{\theta F}$ and compression/extension k_F are also taken into account along Eq. (6) [16].

$$\begin{cases} \theta_F = \frac{L+l}{L} \cdot \frac{\sqrt{2R_F}}{0.093Ewt^{2.5}}M_J = \frac{1}{k_{\theta F}}M_J \\ z_F = \frac{\sqrt{2R_F}}{0.48Ewt^{0.5}}F_J = \frac{1}{k_F}M_J \end{cases} \qquad (6)$$

Load conditions also deform each flexure joint. The resulting angular deformation of a single flexure can be described according to Eq. (7).

$$\theta_J = \frac{l}{EI}\left(1 + \frac{l}{2L}\right)M_J = \frac{1}{k_{\theta J}}M_J, \quad I = \frac{wt^3}{12} \qquad (7)$$

The tensile/compressive deformation is simply described as Eq. (8).

$$z_J = \frac{l}{Ewt}F_J = \frac{1}{k_J}F_J \qquad (8)$$

Additionally, the tensile/compressive compliance of the ground part on which the joints are connected is considered as k_B. Considering the above compliance properties and their layout, definitions for Eq. (2) and (4) can be updated as Eq. (9).

$$\begin{cases} k_\theta = 2\left(\frac{1}{k_{\theta J}} + \frac{1}{k_{\theta F}}\right)^{-1}, \quad \theta = \theta_J + \theta_F \\ k_Z = \left(\frac{2}{k_J} + \frac{1}{k_P} + \frac{2}{k_F} + \frac{1}{k_B}\right)^{-1}, \quad z = 2z_J + z_P + 2z_F + z_B \end{cases} \qquad (9)$$

Force completeness, the buckling shape of the actuator is first mode. In the case, beam flexures are allow buckling only in their first mode whose conditions are that one end is fixed and another is free. By the end conditions, the maximal axial force exerted on the flexures, F_P, must be less than the critical buckling force of the beam flexures, F_B, as shown in Eq. (10)

$$F_P \ll F_B = \frac{\pi^2 EI}{(2l)^2} \qquad (10)$$

Note that this analysis assume a point sized keystone, and motion constrained in the in the y direction.

Preloading

Because PZT stack layers may delaminate when cycled under tensile loads, PZT stacks should not be placed in tension.

However, compressively preloading the stacks with another material (as shown in Fig. 5) allows for the assembled actuator unit to be placed in tension up to the force of the preload without placing the stacks themselves in tension. With the capability of generating tensile force, the output energy per cycle of the actuator is greatly increased. The most significant drawback, however, is the reduction of displacement due to the added stiffness of the preloading material to the coefficient of the piezoelectric actuator in Eq. (9). Therefore it is desirable to reduce the stiffness of the preloading material while increasing the force.

We use a super-elastic type of SMA, however, the super elasticity is not why SMA is used. It has the property of having a super elastic region of near zero stiffness in the stress-strain relationship, but the phenomenon occurs only in cases of larger strain variation that are typically around 4%. Figure 5 shows an experimental setup of a buckling actuator, in which SMA wires are placed in parallel with each of two piezoelectric stacks. Due to the small strain of the piezoelectric stacks, the super-elastic region of the SMA is not used. As a result, the equivalent stiffness of SMA is almost the same as regions other than the super-elastic region shown in Fig.6 where the solid line curves are roughly equal in modulus. Because of the low operating maximum piezoelectric strain of almost 0.1% of maximum piezoelectric strain, the operating SMA stress amplitude is low, around ±10 MPa. This allows for utilization of the SMA high stress region around 800MPa with about 7% strain of the SMA [17]. In this condition, the modulus/stress ratio becomes 25[Pa/Pa] which is almost ¼ of Beryllium copper, a common flexure material due to this property [18]. This usage of SMA as a simple preloading mechanism as shown in Fig. 5 contributes a negligibly low stiffness, which is less than 2% of a piezoelectric stack, and provides a high preloading force equal to the blocking force of the piezoelectric stack. Furthermore, the slight energy loss due to hysteresis of the SMA is estimated to 6.7 [mJ] basing on the experimental result shown in Fig. 6, which is significantly less than the gain of the full "push-pull" energy output of the PZT stack of 113.4 [mJ].
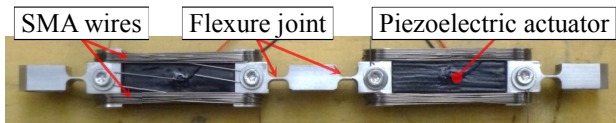

FIGURE 5. FABRICATED BUCKLING UNIT APPLYING SMA PRELOADING

Stresses

The maximum stress generated in the joints by the load condition described above is located on the joint surface connection point between the filets and flexure beams. The stresses at these points are described in Eq. (11).

$$\sigma_{Jmax} = \frac{1}{wt} F_J \pm \frac{6(L+2l)}{lwt^2} M_J \qquad (11)$$

Eq. (11) shows that the stress depends on both force and displacement of the buckling actuator.

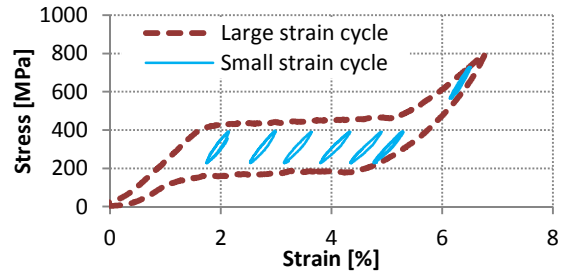FIGURE 6. EXPERIMENTAL RESULTS OF THE STRESS-STRAIN RELATIONSHIP OF SMA FOR NARROW STRAIN MOTION

Force and stress properties

Using Eq. (3), (8) and (9), the force-displacement relationship and the stress-displacement relationship of the flexure buckling actuator is described as Fig. 7. Figure 7 shows only positive region for y. The force in the negative y region is symmetric with respect to the origin. If the bending load generates a tensile stress on a surface in the positive y region, then it works as compressive stress in the negative y regions. The compressive/tensile load works similarly in both positive and negative regions of y. As a result, the stress on a surface which is the tensile by the bending load in positive y region, has the symmetric property around the y=0 axis of the stress which is compressive in bending in the positive y region.
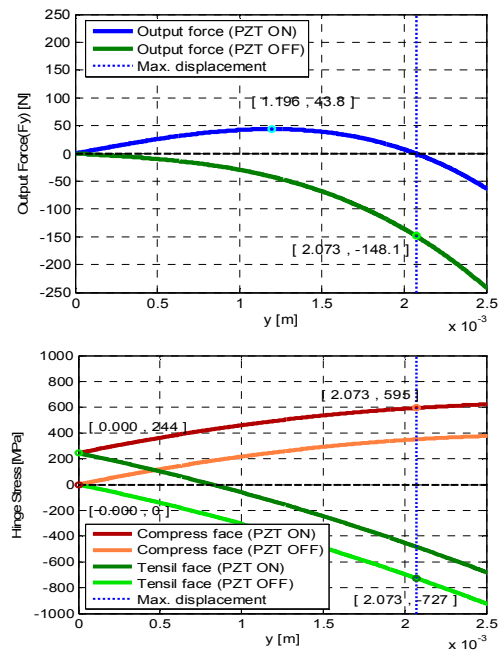

FIGURE 7. FORCE-DISPLACEMENT AND STRESS-DISPLACEMENT REALTIONSHIPSFOR A BUCKLING ACTUATOR (A DESIGN CALCULATION)

4

Validation by FEA

Table 1 shows typical values of both FEA and the design calculation (DCal) shown above. All differences between FEA and DCal are less than 13%, which ensures that the simplified model used for DCal represents well the dominant physical properties of buckling actuators. Surface stresses of FEA are mean values in surfaces of beam for the purpose of not focus on singular values depending on stress concentrations.

TABLE 1. COMPARISON BETWEEN DESIGN CALCULATION AND FEA

		Design calculation	Structural analysis	
			Value	Error rate
Max. displacement [mm]@150[V]		2.073	1.857	12%
Output force	150[V], y=1.2[mm]	43.8	50.2	-13%
	0[V], y=2.1[mm]	153.0	158.4	-3%
Surface stress [MPa] @150[V], y=2.1[mm]	Compress by bend	598	580	3%
	Stretch by bend	495	532	-7%
Surface stress [MPa] @0[V], y=2.1[mm]	Compress by bend	354	374	-5%
	Stretch by bend	739	723	2%

Shape optimization

Important properties of displacement amplification mechanism include maximum force, maximum displacement, and energy efficiency. The main design restriction of the mechanism is to ensure the flexures do not fail from fatigue, and to a lesser extent, do not plastically yield in the short term. The amplification ratio, which is described by the ratio between input and output displacement in the case of a linear transformation, is highly affected by the geometry of the mechanism, mainly the length of the solid body, L. This is similar to the strong dependence on arm length in lever based mechanisms. Additionally, for a given length, L, the flexure properties affect the output properties including the energy transfer efficiency, R_E, which is defined by Eq. (12). Greater R_E yields higher output force for the same maximum displacement.

$$R_E = \frac{E_{out}}{E_{in}}$$
$$\begin{cases} E_{out} = \int_0^{y_{max}} yF(y)|_{F_P=F_{Pblock}}\, dy - \int_0^{y_{max}} yF(y)|_{F_P=0}\, dy \\ E_{in} = z_{Pfree}F_{Pblock} \end{cases}$$
$$(12)$$

In Eq. (12), E_{in} is the maximum output energy from the piezoelectric stack with the ideally preloaded mechanism which is the integral over both the push and pull actuation. E_{out} is the maximum output energy from the buckling actuator which

is the integral over both the push and pull actuation from the maximum actuation of the piezoelectric stack.

Figures 8 and 9 show both R_E and the maximum stress amplitude of the flexures with respect to both length and thickness of the flexure beams. The calculation parameter values are shown in Tab. 2. The maximum stress amplitude is calculated for the case of a single directional actuation of the buckling actuator. Due to complexity of Eq. (4) with respect to y, it is impractical to maximize R_E analytically. For this reason, we obtain the thickness and the length of the beam flexures, which maximize R_E considering the allowable stress amplitude, by referring the analytical results presented in Fig. 9.
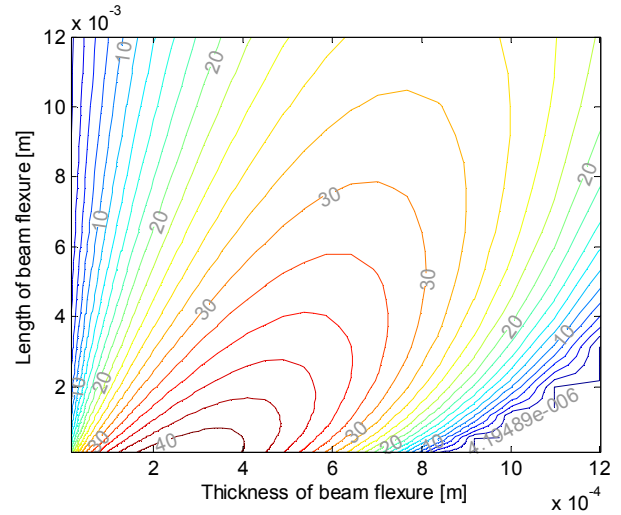

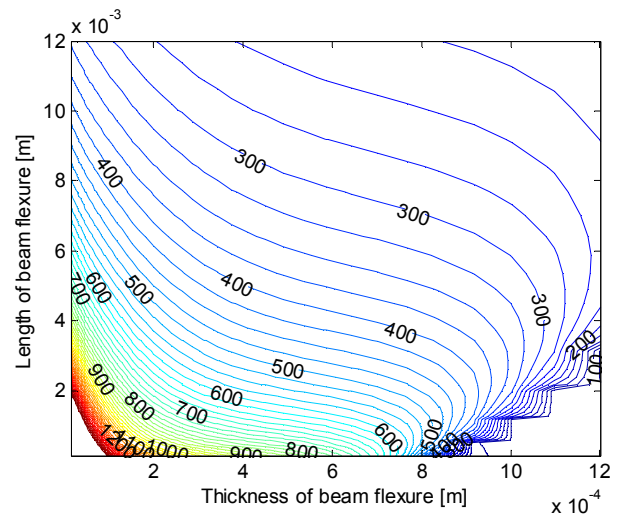FIGURE 8. ENERGY COUPLING RATIO [%] OF BUCKLING MECHANISM WITH RESPECT TO FLEXURE FEATURES

FIGURE 9. MAXIMUM STRESS AMPLITUDE IN SURFACES OF FLEXURE [MPA] WITH RESPECT TO FLEXURE FEATURES

5

TABLE 2. CONDITIONS OF DCAL FOR FIG. 8 AND 9

Piezo-electric actuator	Dimensions	mm	10 x 10 x 36
	Blocking force	N	5400
	Free displacement	μm	42
Flexures	Width	mm	15
	Radii of filets	mm	2
	Material		440C stainless steel

EXPERIMENTAL EVALUATION OF THE BUCKLING ACTUATOR

Figures 10 and 11 show the force-displacement relationship obtained by both prototype experiments and calculations. During experimental evaluation, the keystone was constrained to move in one dimension, without which an unconstrained keystone may rotate. In these calculations, the blocking force of the piezoelectric stack with SMA preloading is assumed to be the same as the specification of the piezoelectric stack alone. This is because preloading has the potential to enhance the piezoelectric property in such a preload range. Without this assumption, the displacement measured experimentally becomes nearly 2.5% larger than the calculation result. With this assumption, the results of both experiments and calculations fit each other well.

12N of hysteresis arises in both experimental results, which is estimated to be caused by the yield deformation of flexures, not by hysteresis of the piezoelectric stacks because same phenomenon happens if aluminum bars are used instead of the piezoelectric stacks. The flexures are made by 440C stainless steel but are not annealed properly, which varies the yield strength to less than 600MPa. Due to the hysteresis, it is hard to find a position where the buckling actuators become flat. Hence, the original positions in the figures are placed in one of stable positions with applying maximum voltage to piezoelectric stacks in Fig. 10.

PIEZOELECTRIC BRAKE

Implementation design of a piezoelectric brake actuator

Using the buckling actuators shown above, we designed a brake actuator to be attached to a commercial EM motor. The outline of the structure is shown as Fig. 12 and the implementation design is shown in Fig. 13. Many brakes for commercial EM motors are usually required to have "Normally ON" function, which means that brakes must hold the rotor of the motor without a power supply. To obtain enough force for the function, coil springs are added in parallel with the buckling actuators. The center parts of buckling actuators can easily rotate without any linear guide around the perpendicular axis to both y and z, which severely impair the output force. Three buckling actuators arranged as in Fig. 13 can restrict the rotation of each other by their high rotational stiffness around

each z axis. They also bear the brake torque which is much smaller force along z axis than the piezoelectric force.

The flexures are designed to maximize the brake stroke which means the displacement range where the holding force, including the additional springs, is greater than a design specification.
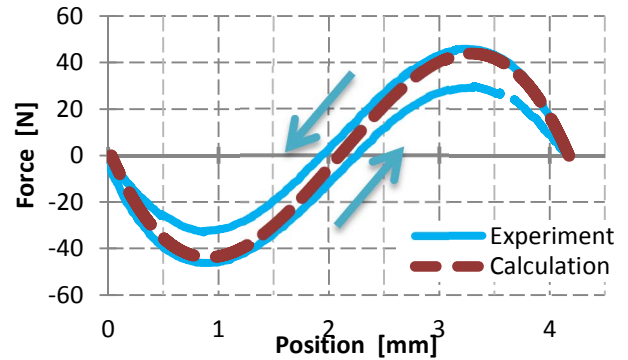

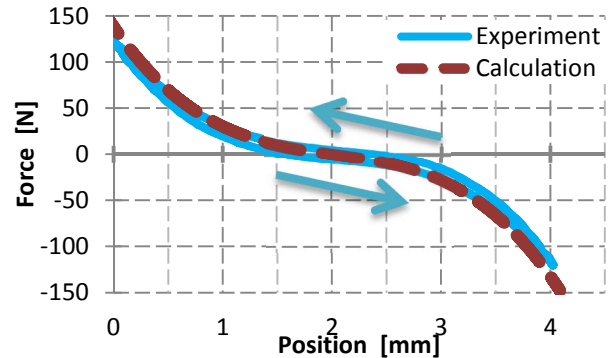FIGURE 10. EXPERIMENTAL RESULT OF FORCE – DISPLACEMENT PROPERTY IN COMPRESSIONAL ACTUATION

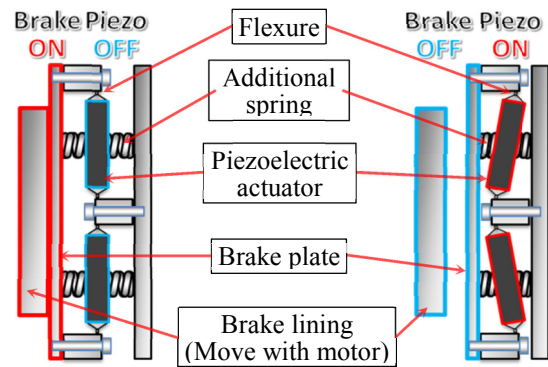FIGURE 11. EXPERIMENTAL RESULT OF FORCE – DISPLACEMENT PROPERTY IN TENSILE ACTUATION

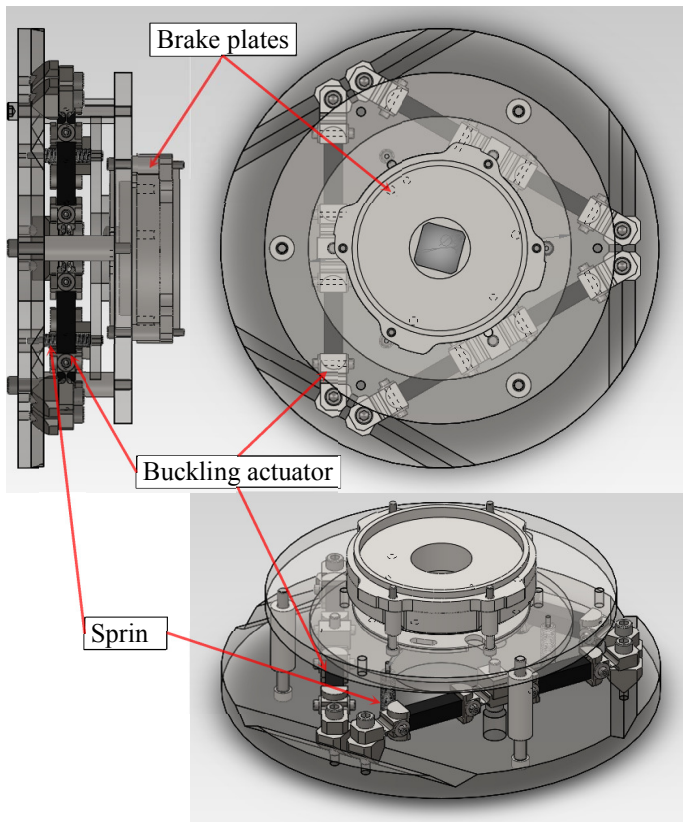FIGURE 12. BASIC ARCHITECTURE OF PIEZOELECTRIC BRAKE

Copyright © 2012 by ASME

FIGURE 13. FABRICATION MODEL OF PIEZOELECTRIC BRAKE

Brake properties

Figure 14 shows an experimental brake property, which is brake torque against brake gap. Brake plates have potential to wear when slip happens between them. For this reason, actuators for commercial brakes are required to generate holding force in specific ranges. The brake used in the experiment requires 0.3mm as the range in addition to an initial gap whose purpose is to keep brake plates separated from each other. Considering the gap margin, the experimental results show the buckling actuators can apply 2.5Nm of braking torque.

Energy consumption

Figure 15 shows the experimental result of energy consumption. Piezoelectric stacks have a capacitive property in the electric domain and an elastic property in mechanical domain which also performs as capacitive energy storage. To output mechanical energy as an actuator, energy must be stored in both electric and mechanical capacitance. For this basic property of piezoelectric actuators, buckling actuators only consume the energy lost in piezoelectric stacks as hysteresis loss as shown as light blue line in Fig. 15. The result shows the energy consumption in all piezoelectric stacks used in the brake actuator for 20 on-off cycle operations over 100sec. The dark

red line shows the energy input to the piezoelectric stacks which shows 21.3mJ is required for 20 operations. On the other hand, the energy loss in the piezoelectric stacks becomes only 4.7mJ for 20 operations, which can be recovered by applying a charge recycling circuit such, as in [19]. Comparing to the original EM actuator for the brake which requires 19W to release the brake and 950J for half-rate operation, it is assured that the buckling actuator requires much less energy.
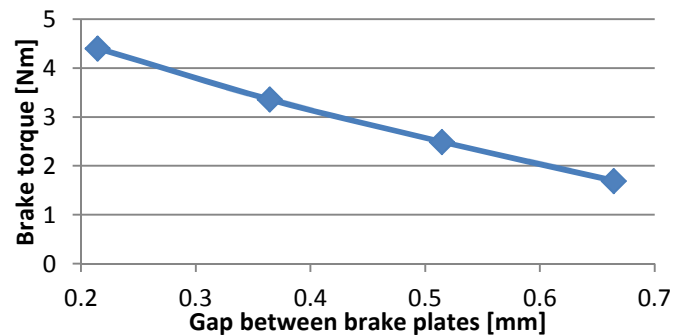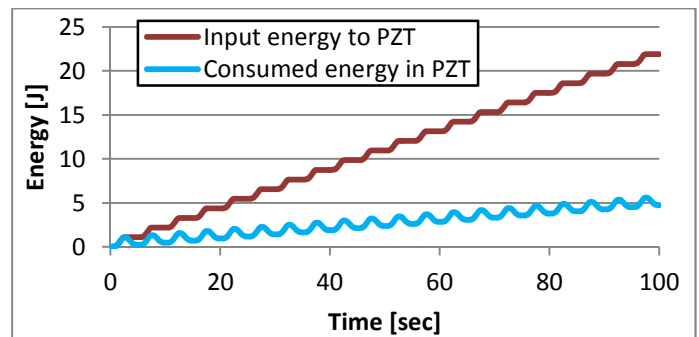

FIGURE 14. BRAKE PROPERTY OF PIEZOELECTRIC BRAKE

FIGURE 15. ENERGY CONSUMPTION OF PIEZOELECTRIC BRAKE

CONCLUSION

An analytic method for designing buckling actuators using flexure joints is presented. The method is evaluated by FEA and the result shows less than 13% error in force and displacement. Prototype experimental result also fit well with the design calculation. A preloading mechanism employing SMA is applied and performs as an almost zero stiffness load which provides the same force as the blocking force of the piezoelectric stack. The integrated experimental apparatus performs the complete push-pull feature while thoroughly utilizing of the potential of piezoelectric actuators.

The buckling actuators are applied as a brake for a commercial motor, and deliver holding force which generates more than 2.5Nm of brake torque in the range of the gap

Copyright © 2012 by ASME

between brake plates from 0.2mm to 0.5mm. The energy consumed for the brake operation is significantly lower than the EM motor originally used for the brake.

These results show the remarkable properties of the piezoelectric driven buckling actuator and assist in broadening the range of applications of motors driven by them.

REFERENCES

[1]   H. P. Huy, "Design and simulation of micro-linear actuator," in *2010 IEEE Conference on Robotics Automation and Mechatronics (RAM)*, 28-30 June 2010.

[2]   Y. Taiho, S. W. Terrence, Z. Min, N. T. Mark and C. Tiahong, "High frequency, large displacement, and low power consumption piezoelectric translational actuator based on an oval loop shell," *Sensors and Actuators A: Physical, Volume 176,* pp. 99-109, April 2012.

[3]   P. Mottard and Y. St-Amant, "Analysis of flexural hinge orientation for amplified piezo-driven actuators," *Smart Materials and Structures,* vol. Volume 18 Number 3, January 2009.

[4]   H.-W. Ma, S.-M. Yao , L.-Q. Wang and Z. Zhong, "Analysis of the displacement amplification ratio of bridge-type flexure hinge," *Sensors and Actuators A: Physical,* vol. 132, no. 2, pp. 730-736, 20 November 2006.

[5]   E. Furukawa, M. Mizuno and T. Doi, "Development of a Flexure-Hinged Translation Mechanism Driven by Two Piezoelectric Stacks," *JSME international journal. Ser. C, Dynamics, control, robotics, design and manufacturing,* Vols. 38-C(4), pp. 743-748, 12-15-1995.

[6]   T. Secord and H. Asada, "Scaling Analysis for Large Stroke Piezoelectric Actuators," in *Proc. of IFAC Symposium on Mechatronic Systems*, September 2010.

[7]   I. Hayashi, N. Iwatsuki, M. Kawai, J. Shibata and T. Kitagawa, "Development of piezoelectric cycloid motor," in *Robot Actuators, IEE Colloquium on*, Oct 1991.

[8]   D. Neal and H. Asada, "Dynamic Performance of Nonlinear 100x Displacement Amplification Piezoelectric Actuator," in *Proc. of 2010 ASME Dynamic Systems and Control Conference*, September 2010.

[9]   J. Torres, H. Asada and D. Neal, "A PZT Array Actuator Using Buckling Strain Amplification and Preload Mechanisms," in *Proc. Of 2011 ASME Dynamic Systems and Control Conference*, Oct. 31-Nov.2, 2011.

[10]   P. M. Chaplya, M. Mitrovic, G. P. Carman and F. K. Straub, "Durability properties of piezoelectric stack actuators under combined electromechanical loading," *JOURNAL OF APPLIED PHYSICS,* vol. 100, 29 December 2006.

[11]   Q. Zhang and J. Zhao, "Electromechanical properties of lead zirconate titanate piezoceramics under the influence of mechanical stresses," *Ultrasonics, Ferroelectrics and Frequency Control, IEEE Transactions on,* vol. 46, no. 6, pp. 1518-1526, Nov. 1999.

[12]   B. Cook, J. Koenig, D. Braun, D. Moore and S. Hankins, "Direct Drive Precision Linear Actuator for Space Interferometry Mission (SIM) Siderostat Pointing," in *Aerospace Conference, 2008 IEEE*, March 2008.

[13]   M. Gogola and M. Goldfarb, "Design of a PZT-actuated proportional drum brake," *Mechatronics, IEEE/ASME Transactions on,* vol. 4, no. 4, pp. 409-416, Dec 1999.

[14]   G.-W. K. a. K. W. Wang, "Piezoelectric-hydraulic pump based band brake actuation system for automotive transmission control," *Proc. SPIE,* 2007).

[15]   B. A. a. R. H. C. Mangeot, "New actuators for aerospace," 2009. [Online]. Available: http://www.noliac.com/New_diamond_actuators_for_ae rospace-8349.aspx.

[16]   Y. K. Yong and T.-F. Lu, "Comparison of circular flexure hinge design equations and the derivation of empirical stiffness formulations," *Advanced Intelligent Mechatronics, 2009. AIM 2009. IEEE/ASME International Conference,* pp. 510-515, 14-17 July 2009.

[17]   A. Pelton, "Nitinol Fatigue: A Review of Microstructures and Mechanisms," *Journal of Materials Engineering and Performance,* vol. 20, no. 4-5, pp. 613-617 , July 2011.

[18]   S. T. Smith, Flexures: elements of elastic mechanisms, CRC Press, Aug 8, 2000.

[19]   P. T. S. a. A. H. Barragán, "Design of Energy-Saving PZT Drive Amplifiers For Mobile And Wearable Physical Assists," in *Proc. Of 2011 ASME Dynamic Systems and Control Conference*, 2011.

[20]   J. Ueda, T. Secord and H. Asada, "Large Effective-Strain Piezoelectric Actuators Using Nested Cellular Architecture With Exponential Strain Amplification Mechanisms," *IEEE/ASME Transactions on Mechatronics,* Vols. 15, no.5, pp. 770-782, Oct. 2010.

[21]   K. Yamatoh, M. Ogura, K. Kanbe and Y. Isogami, "Piezoelectric brake device". USA Patent 4854424, 8 Aug. 1989.

[22]   J. Samuel Allen Face, "Anti-lock brake system with piezoelectric brake actuator". USA Patent 6213564, 10 Apr. 2001.

[23]   X.-Y. G. a. T. D. Alan R. Pelton, "FATIGUE TESTING OF DIAMOND-SHAPED SPECIMENS," in *SMST-2003: proceedings of the international conference on shape memory and superelastic technologies*, 2003.